# Near-Infrared Circular Dichroism, Magnetic Circular Dichroism, and X-ray Absorption Spectral Comparison of the Non-Heme Ferrous Active Sites of Plant and Mammalian 15-Lipoxygenases

**Mark A. Pavlosky,[†] Yan Zhang,[‡] Tami E. Westre,[†] Qing-Fen Gan,[‡] Elizabeth G. Pavel,[†] Cecelia Campochiaro,[†] Britt Hedman,[†,§] Keith O. Hodgson,[†,§] and Edward I. Solomon*,[†]**

*Contribution from the Department of Chemistry and Stanford Synchrotron Radiation Laboratory, Stanford University, Stanford, California 94305, and the Institute of Biochemistry and Cell Biology, Syntex Discovery Research, Palo Alto, California 94304*

*Received October 25, 1994*[⊗]

**Abstract:** Lipoxygenases (LOs) are non-heme iron enzymes which catalyze the reaction of dioxygen with *cis,cis*-1,4-pentadiene-containing fatty acids to form hydroperoxide products, which in mammals are the precursors to the inflammation- and immunity-mediating compounds lipoxins and leukotrienes. Recent X-ray crystal structures of ferrous soybean lipoxygenase-1 (SLO-1) offer two different descriptions of the active site: one four-coordinate and one five- or six-coordinate. Near-infrared (NIR) circular and magnetic circular dichroism (CD/MCD) and variable-temperature, variable-field (VTVH) MCD have been used to study SLO-1 in solution which is found to exist as a 40/60% mixture of five- and six-coordinate forms, respectively. Addition of linoleate substrate or alcohols shifts the mixture to the purely six-coordinate form. NIR CD/MCD studies of two mammalian LOs, rabbit reticulocyte and recombinant human 15-LOs, show that these exist as pure six-coordinate forms. X-ray absorption Fe K-edge and pre-edge data also show that the mammalian 15-LOs and SLO-1 in glycerol are six-coordinate. This is consistent with the extended X-ray absorption fine structure (EXAFS) results of SLO-1 in glycerol which show the iron active site to have 5 ± 1 N/O at ~2.16 Å. VTVH MCD data on the six-coordinate sites show that the mammalian and soybean enzymes have very different ground-state splittings, indicative of differences in bonding interactions with the ligand set. These differences in ferrous site coordination in solution and ground-state splittings are attributed to the substitution of a stronger histidine ligand in the mammalian 15-LOs for an asparagine in SLO-1.

## Introduction

Lipoxygenases (LOs) are non-heme iron enzymes which catalyze the reaction of dioxygen with *cis,cis*-1,4-pentadiene-containing fatty acids, *e.g.*, linoleic and arachidonic acids, to form hydroperoxide products. Certain LOs are positionally specific and are classified by the carbon position at which the hydroperoxidation of arachidonic acid occurs. Mammalian 5-, 12-, and 15-LOs catalyze the formation of the direct precursors to leukotrienes and lipoxins,[1] compounds which mediate inflammation, hypersensitivity, and cellular immunity. LOs have also been implicated in the oxidation of low-density lipoprotein to its atherogenic form.[2,3] Thus, the development of LO inhibitors has been the target of many pharmaceutical companies. In plants, LOs are involved in immunity and growth regulation.[4] Soybean lipoxygenase-1 (SLO-1) and mammalian 5- and 15-LOs have regions of high amino acid sequence identity.[5] Maximal alignment of the LOs shows that the middle and COOH terminal portions are very similar. The nonhomology of the first 117 residues of SLO-1 (MW ~95 000) with the mammalian LOs (MW ~75 000) is thought to be due to an additional region present only in plant LOs.[5,6]

SLO-1, a 15-LO, catalyzes the reaction of $O_2$ with linoleic acid to give primarily 13(*S*)-hydroperoxy-9,11(*E,Z*)-octadecadienoic acid (13-HPOD) as product. The native ferrous enzyme is stable in air[7] and must be oxidized to the active ferric form for reaction with substrate. There are two classes of proposed mechanisms for LO catalysis. The first is a radical-based mechanism in which the fatty acid is activated through oxidation by the ferric center to form a fatty acid radical.[8,9] The ferrous site generated may then activate $O_2$ for reaction with the radical, or $O_2$ may react with the radical to generate product. The second mechanism involves a direct reaction of the ferric center and the substrate, forming an organo-iron complex[10] to which $O_2$ inserts, forming a ferric peroxo complex and subsequently product.

Two recent X-ray crystal structures[6,11] of ferrous SLO-1 have identified four common amino acid active site ligands: histidine$_{499}$N$\epsilon$, histidine$_{504}$N$\epsilon$, histidine$_{690}$N$\epsilon$, and isoleucine$_{839}$OT2,

* To whom correspondence should be addressed.
† Department of Chemistry, Stanford University.
‡ Syntex Discovery Research.
§ Stanford Synchrotron Radiation Laboratory, Stanford University.
⊗ Abstract published in *Advance ACS Abstracts,* April 1, 1995.

(1) Samuelsson, B.; Dahlén, S.-E.; Lindgren, J. Å.; Rouzer, C. A.; Serhan, C. N. *Science* **1987**, *237*, 1171.
(2) Sigal, E.; Laughton, C. W.; Mulkins, M. A. *Ann. N. Y. Acad. Sci.* **1994**, *714*, 211.
(3) Steinberg, D.; Parthasarathy, S.; Carew, T. E.; Khoo, J. C.; Witztum, J. L. *N. Engl. J. Med.* **1989**, *320*, 915.
(4) Gardner, H. W. *Biochim. Biophys. Acta* **1991**, *1084*, 221.
(5) Sigal, E. *Am. J. Physiol.* **1991**, *260*, L13.
(6) Boyington, J. C.; Gaffney, B. J.; Amzel, L. M. *Science* **1993**, *260*, 1482.
(7) Petersson, L.; Slappendel, S.; Vliegenthart, J. F. G. *Biochim. Biophys. Acta* **1985**, *828*, 81.
(8) Veldink, G. A.; Vliegenthart, J. F. G. *Adv. Inorg. Biochem.* **1984**, *6*, 139.
(9) Nelson, M. J.; Cowling, R. A.; Seitz, S. P. *Biochemistry* **1994**, *33*, 4966.
(10) Corey, E. J.; Nagata, R. *J. Am. Chem. Soc.* **1987**, *109*, 8107.
(11) Minor, W.; Steczko, J.; Bolin, J. T.; Otwinowski, Z.; Axelrod, B. *Biochemistry* **1993**, *32*, 6320.

0002-7863/95/1517-4316$09.00/0 

the terminal carboxylate. Each of these residues is conserved in all sequenced lipoxygenases, with the exception of a valine replacement of the isoleucine in rat leukocyte 5-LO.[12] One crystallographic active site description is four-coordinate distorted octahedral with two adjacent unoccupied ligand positions.[6] The other crystal structure[11] has an additional ligand, asparagine$_{694}$O$\delta$1, with the further possibility of a sixth water-based ligand; such a ligand has been proposed from electron paramagnetic resonance (EPR) line broadening studies on the ferric enzyme.[13] This asparagine residue is conserved in all sequenced LOs with the exception of rabbit reticulocyte and human 15-LOs, in which a histidine is in the analogous position.[5]

There have been a limited number of spectroscopic studies aimed at defining the geometric and electronic structure of the ferrous site of SLO-1. Magnetic susceptibility measurements[7] show that the ferrous active site ground state is high-spin with $S = 2$. X-ray absorption,[14] Mössbauer,[15] and circular and magnetic circular dichroism[16] (CD/MCD) studies predicted a distorted octahedral geometry; however, these studies now appear to have been complicated by solvent effects. Recently we communicated[17] a CD/MCD study in the near-infrared (NIR) region on native SLO-1 in solution using sucrose as a nonperturbing low-temperature glassing agent, which showed that native ferrous SLO-1 exists as a mixture of two forms, one five-coordinate and one six-coordinate, and that the addition of glycerol converts the mixture to the pure six-coordinate form.

We have now extended our ferrous NIR CD/MCD studies of the two native SLO-1 forms to include variable-temperature, variable-field (VTVH) MCD data and ground-state analyses, small molecule interactions, and ligand field calculations to model the electronic structure. This protocol has been further applied to two mammalian LOs, rabbit reticulocyte 15-LO (15-RLO) and recombinant human 15-LO (15-HLO). X-ray absorption spectroscopy (XAS) has also been employed to compare the mammalian 15-LOs to the pure native SLO-1 form in glycerol. It is found that, in contrast to the plant 15-LO SLO-1, the mammalian 15-LOs exist as one form with a six-coordinate ferrous active site, and analysis shows that these have different ground-state spin Hamiltonian parameters. These active site geometric and electronic structure differences can be attributed to ligand substitution of Asn$_{694}$ in SLO-1 by histidine in the mammalian 15-LOs.

## Experimental Section

SLO-1 was purified from soybeans (Williams Variety, Tabor Seed Division) following published procedures.[18] The specific activity of the final enzyme was ~200 units/mg. Native SLO-1 samples were buffered in 0.1 M deuterated sulfonic acid solutions: MES, 5.6 < pD < 7; HEPES, 7.5 < pD < 8.2; CHES, 8.5 < pD < 9.5; CAPS, 10 < pD < 11. MCD samples used either 50% (v/v) glycerol-$d_3$ or were saturated with sucrose for low-temperature glassing. A 2-fold excess of sodium dithionite was added to the samples involving linoleate to remove $O_2$, to reduce any ferric enzyme present, and to reduce a <1% heme impurity. Sodium linoleate (99%, Sigma) was dissolved in the 0.1 M pD 9.2 CHES buffer with ~25 mM Tween 20 (ICN Biochemicals) as a solubilizing agent. Sodium dithionite and/or Tween 20 cause no change in the NIR CD spectrum of native SLO-1. Human 15-LO was purified from a baculovirus/insect cell expression system by anion-exchange chromatography on a Mono Q column.[19] Rabbit 15-LO was purified from a 55% ammonium sulfate precipitate of rabbit reticulocyte lysate to greater than 98% purity according to the published method with the following modifications: desalting the protein with a PD-10 column instead of dialysis and replacement of the Mono S with a Mono Q column.[20]

NIR CD and MCD spectroscopies were performed on a Jasco J200D spectropolarimeter (600−2150 nm) equipped with an Oxford Instruments SM4-7T superconducting magnet. CD spectra were obtained from samples in a 1 cm path length cell at 3 °C, and MCD spectra were obtained from 3 mm thick samples as described previously.[21] The depolarization of the samples was checked by measuring the CD of a freshly prepared nickel tartrate solution placed immediately before and after the sample,[22] and the samples exhibited <5% depolarization at 4.2 K. CD and MCD spectra were fit to Gaussian band shapes using a Levenberg/Marquardt method.

X-ray absorption spectra were recorded at the Stanford Synchrotron Radiation Laboratory on unfocused beamline 7-3 during dedicated conditions (3 GeV, 50−100 mA). The radiation was monochromatized using a Si(220) double-crystal monochromator. An Oxford Instruments continuous-flow liquid helium CF1208 cryostat was used to maintain a constant temperature of 10 K. Energies were calibrated using an internal Fe foil standard, assigning the first inflection point to 7111.2 eV.[23] The spectrometer energy resolution was approximately 1.5 eV with reproducibility in edge position determination of <0.2 eV.

The SLO-1, 15-RLO, and 15-HLO XAS samples were prepared as described above with 50% glycerol. The samples were loaded into Lucite XAS cells (23 × 1 × 3 mm) with 37 $\mu$m Kapton windows and frozen in liquid nitrogen. Data were measured to $k = 13$ Å$^{-1}$ with 1 mm high premonochromator beam defining slits, detuning the monochromator 50% at 7824 eV to minimize harmonic contamination. The fluorescence signal was monitored by using a 13-element Ge solid-state array detector[24] windowed on the Fe K$\alpha$ signal. During the experiment, count rates of approximately 30 000 s$^{-1}$ total per element were not exceeded. Approximately 30 scans were averaged for each protein sample. A pre-edge subtraction was performed by fitting the tail of a Gaussian to the pre-edge region and subtracting this polynomial from the averaged spectra.[25] A three-segment spline approximately even in $k$-space was fit to the extended X-ray absorption fine structure (EXAFS) region, and the data were normalized to an edge jump of 1 at 7130 eV. The spline was chosen so that it minimized residual low-frequency background but did not reduce the EXAFS amplitude as checked by monitoring the Fourier transform of the EXAFS during the background subtraction process.

Fe K-edge spectra were also collected on four-, five-, and six-coordinate ferrous model complexes. Fe(HB(3,5-$i$Pr$_2$pz)$_3$)Cl[26] and [Fe(trpn)(MeCN)](CF$_3$SO$_3$)$_2$[27] were obtained as gifts from N. Kitajima and K. Hagen, respectively.[28] [Fe(imidazole)$_6$]Cl$_2$[29] was prepared as previously described. These three samples are air-sensitive, and thus the following procedure was carried out in a nitrogen-filled glovebox. The crystalline samples were each mixed with BN and ground into a

(12) Sigal, E.; Craik, C. S.; Highland, E.; Grunberger, D.; Costello, L. L.; Dixon, R. A. F.; Nadel, J. A. *Biochem. Biophys. Res. Commun.* **1988**, *157*, 457.
(13) Nelson, M. J. *J. Am. Chem. Soc.* **1988**, *110*, 2985.
(14) Van der Heijdt, L. M.; Feiters, M. C.; Navaratnam, S.; Nolting, H.-F.; Hermes, C.; Veldink, G. A.; Vliegenthart, J. F. G. *Eur. J. Biochem.* **1992**, *207*, 793.
(15) Dunham, W. R.; Carroll, R. T.; Thompson, J. F.; Sands, R. H.; Funk, M. O., Jr. *Eur. J. Biochem.* **1990**, *190*, 611.
(16) Whittaker, J. W.; Solomon, E. I. *J. Am. Chem. Soc.* **1988**, *110*, 5329.
(17) Pavlosky, M. A.; Solomon, E. I. *J. Am. Chem. Soc.* **1994**, *116*, 11610.
(18) Nelson, M. J. *Biochemistry* **1988**, *27*, 4273.
(19) Kühn, H.; Barnett, J.; Grunberger, D.; Baeker, P.; Chow, J.; Nguyen, B.; Bursztyn-Pettegrew, H.; Chan, H.; Sigal, E. *Biochim. Biophys. Acta* **1993**, *1169*, 80.
(20) Sloane, D. L.; Browner, M. F.; Dauter, Z.; Wilson, K.; Fletterick, R. J.; Sigal, E. *Biochem. Biophys. Res. Commun.* **1990**, *173*, 507.
(21) Pulver, S.; Froland, W. A.; Fox, B. G.; Lipscomb, J. D.; Solomon, E. I. *J. Am. Chem. Soc.* **1993**, *115*, 12409.
(22) Browett, W. R.; Fucaloro, A. F.; Morgan, T. V.; Stephens, P. J. *J. Am. Chem. Soc.* **1983**, *105*, 1868.
(23) Scott, R. A.; Hahn, J. E.; Doniach, S.; Freeman, H. C.; Hodgson, K. O. *J. Am. Chem. Soc.* **1982**, *104*, 5364.
(24) Cramer, S. P.; Tench, O.; Yocum, M.; George, G. N. *Nucl. Instrum. Methods Phys. Res.* **1988**, *A266*, 586.
(25) George, G. N.; Pickering, I. To be published.
(26) Kitajima, N. Private Communication.
(27) Hagen, K. Private communication.
(28) Abbreviations used: HB(3,5-$i$Pr$_2$pz)$_3$ = hydrotris(3,5-diisopropyl-1-pyrazolyl)borate; trpn = (NH$_2$CH$_2$CH$_2$CH$_2$)$_3$N.
(29) Burbridge, C. D.; Goodgame, D. M. L. *Inorg. Chim. Acta* **1970**, *4*, 231.

fine powder. The BN/sample mixture was pressed into a 1 mm thick Al spacer that was sealed with 63.5 $\mu$m Mylar tape windows. Data were measured in transmission mode with $N_2$-filled ionization chambers to $k$ = 9.5 Å$^{-1}$, detuning the monochromator 50% at 7474 eV to minimize harmonic contamination. Two to three scans were averaged for each sample. A smooth pre-edge background was removed from the averaged spectra by fitting a first-order polynomial to the pre-edge region and subtracting this polynomial from the entire spectrum. A two-segment spline of order 2 was fit to the EXAFS region, and the data were normalized to an edge jump of 1 at 7130 eV.

EXAFS data reduction was performed on the normalized protein spectra according to established methods.[30-32] The normalized data were converted to $k$-space. The photoelectron wave vector, $k$, is defined by $[2m_e(E - E_0)/\hbar^2]^{1/2}$ where $m_e$ is the electron mass, $E$ is the photon energy, $\hbar$ is Planck's constant divided by $2\pi$, and $E_0$ is the threshold energy of the absorption edge, which was defined to be 7130 eV for the Fe K absorption edge. The empirical EXAFS data analyses were performed with nonlinear least-squares curve-fitting[23,30-32] techniques using empirical phase and amplitude parameters. The following models were used to obtain the empirical Fe−X back-scattering parameters of interest: Fe−O from [Fe(acetylacetonate)$_3$][33,34] and Fe−N from [Fe-(1,10-phenanthroline)$_3$](ClO$_4$)$_3$.[35,36] Fourier transforms (from $k$ to R space) were performed for the data range 3.5−12.5 Å$^{-1}$ with a Gaussian window of 0.1 Å$^{-1}$. The window widths used in the back-transforms (from R to $k$ space) are given in the Results and Analysis. The window widths were kept as similar as possible to those used to extract amplitude and phase parameters from the model compounds to minimize artifacts introduced by the Fourier filtering technique. All curve-fitting was based on $k^3$-weighted data and applied to the individual filtered shell of interest. Only the structure-dependent parameters, the distance and Debye−Waller factor, or the distance and coordination number were varied. A "goodness of fit" parameter, $F$, was calculated as $F = \{[k^6(\text{data} - \text{fit})^2]/(\text{no. of points})\}^{1/2}$ for each fit.

The intensities and energies of pre-edge features of the model complex and protein data were quantitated by fits to the data using the fitting program EDG_FIT.[37] All spectra were fit over the range 7108−7118 eV. Pre-edge features were modeled by Voigt line shapes.[38-41] A fixed 50:50 ratio of Lorentzian to Gaussian contribution for the pre-edge feature successfully reproduced these spectral features. The value reported for the area of a fitted feature (where the peak area was approximated by the height × full width at half-maximum) is the average of all the Voigts which successfully fit the feature. For each sample, the standard deviation of the average of the areas was calculated to quantitate the error.

## Results and Analysis

**NIR CD/MCD of SLO-1.** A high-spin ferrous ion ($d^6$ electron configuration) has a $^5$D ground state which is split into a triply degenerate $^5T_{2g}$ ground state and doubly degenerate $^5E_g$ excited state at $10Dq_{O_h}$ higher energy in an octahedral ligand field (LF) (Figure 1A). An octahedral ligand field with biologically relevant N and/or O ligands splits the $^5T_{2g}$ and $^5E_g$

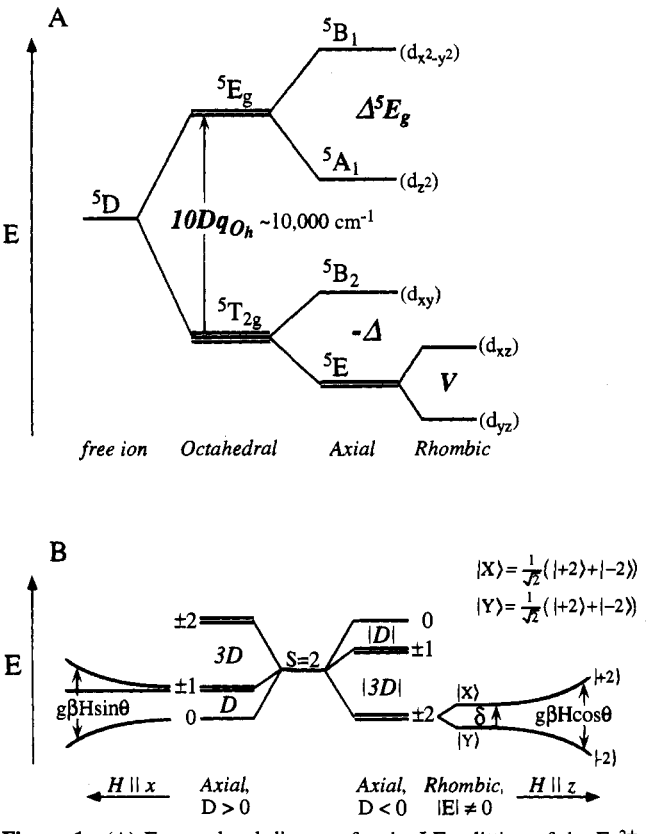


**Figure 1.** (A) Energy level diagram for the LF splitting of the $Fe^{2+}$ quintet ground and excited states in different coordination geometries. These states correspond to having the extra electron of the high-spin $d^6$ configuration occupying the d-orbital indicated in parentheses. (B) Energy level diagram for the quintet ground state with positive (left) and negative (right) axial zero field splitting, rhombic distortion, and applied magnetic field. The wave function changes with magnetic field are also given.

states by ~10 000 cm$^{-1}$. Low-symmetry distortions will further split the $^5E_g$ excited state ($\Delta^5E_g$) by an amount dependent on the coordination geometry. Tetragonal distortion of the octahedral field produces a splitting of the $^5E_g$ excited state of ~2000 cm$^{-1}$,[42-45] centered at ~10 000 cm$^{-1}$. A square pyramidal five-coordinate geometry will split the $^5E_g$ excited state by ≳5000 cm$^{-1}$, the highest energy transition being at ≳10 000 cm$^{-1}$.[46,47] Distortion of the five-coordinate structure along a $C_{2v}$ or $C_s$ coordinate leads to a rhombic splitting and eventually a trigonal bipyramidal geometry. The excited states will still be split by ~5000 cm$^{-1}$; however, this geometry will be experimentally distinct as the highest energy spin-allowed transition will be at <10 000 cm$^{-1}$.[48-50] In addition to the $^5E_g$ splittings, the $^5T_{2g}$ ground state will also undergo splittings dependent on coordination geometry; however, these effects are smaller, <1500 cm$^{-1}$, due to the dependence of the $^5T_{2g}$ set splitting on $\pi$-bonding rather than $\sigma$-bonding interactions of the $Fe^{2+}$ site with the ligands. A tetrahedral ligand environment will split the ferrous

(30) Cramer, S. P.; Hodgson, K. O.; Stiefel, E. I.; Newton, W. E. *J. Am. Chem. Soc.* **1978**, *100*, 2748.
(31) Cramer, S. P.; Hodgson, K. O. *Prog. Inorg. Chem.* **1979**, *25*, 1.
(32) Scott, R. A. *Methods Enzymol.* **1985**, *117*, 414.
(33) Iball, J.; Morgan, C. H. *Acta Crystallogr.* **1967**, *23*, 239.
(34) Roof, R. B., Jr. *Acta Crystallogr.* **1956**, *9*, 781.
(35) Johansson, L. *Chem. Scr.* **1976**, *9*, 30.
(36) Johansson, L.; Molund, M.; Oskarsson, Å. *Inorg. Chim. Acta* **1978**, *31*, 117.
(37) EDG_FIT was written by Dr. Graham N. George of the Stanford Synchrotron Radiation Laboratory.
(38) Agarwal, B. K. *X-ray Spectroscopy*; Springer-Verlag: Berlin, 1979; p 276.
(39) Lytle, F. W.; Greegor, R. B.; Sandstrom, D. R.; Marques, E. C.; Wong, J.; Spiro, C. L.; Huffman, G. P.; Huggins, F. E. *Nucl. Instrum. Methods Phys. Res.* **1984**, *226*, 542.
(40) Lytle, F. W. In *Applications of Synchrotron Radiation*; Winick, H., Xiam, D., Ye, M., Huang, T., Eds.; Gordon and Breach Science Publishers: New York, 1989; p 135.
(41) Tyson, T. A.; Roe, A. L.; Frank, P.; Hodgson, K. O.; Hedman, B. *Phys. Rev. B* **1989**, *39A*, 6305.
(42) Holmes, O. G.; McClure, D. S. *J. Chem. Phys.* **1957**, *26*, 1686.
(43) Cotton, F. A.; Meyers, M. D. *J. Am. Chem. Soc.* **1960**, *82*, 5023.
(44) Goodgame, D. M. L.; Goodgame, M.; Hitchman, M. A.; Weeks, M. J. *Inorg. Chem.* **1966**, *5*, 635.
(45) Loehr, J. S.; Loehr, T. M.; Mauk, A. G.; Gray, H. B. *J. Am. Chem. Soc.* **1980**, *102*, 6992.
(46) Riley, D. P.; Merrell, P. H.; Stone, J. A.; Busch, D. H. *Inorg. Chem.* **1975**, *14*, 490.
(47) Hodges, K. D.; Wollmann, R. G.; Barefield, E. K.; Hendrickson, D. N. *Inorg. Chem.* **1977**, *16*, 2746.
(48) Stoppioni, P.; Mani, F.; Sacconi, L. *Inorg. Chim. Acta* **1974**, *11*, 227.
(49) Chia, P. S. K.; Livingstone, S. E. *Aust. J. Chem.* **1969**, *22*, 1613.
(50) Ciampolini, M.; Nardi, N. *Inorg. Chem.* **1966**, *5*, 1150.

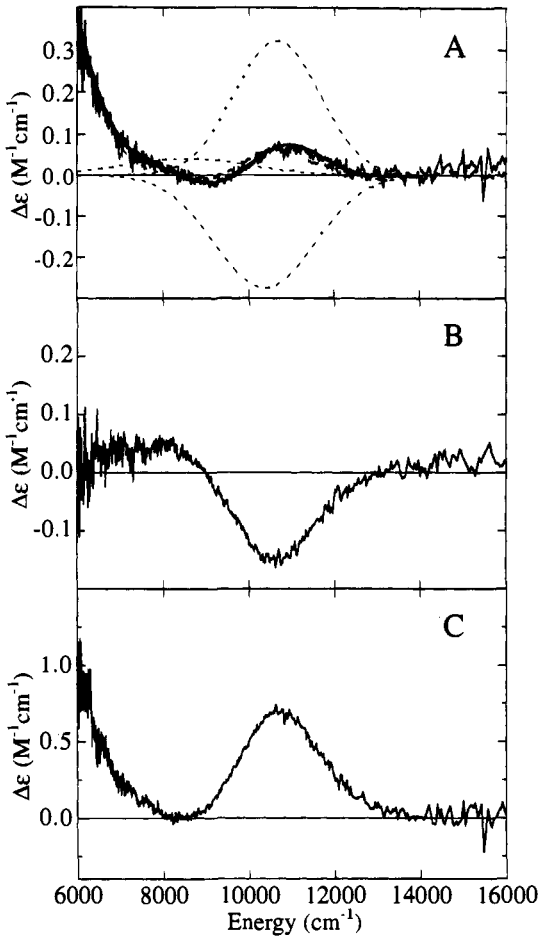


**Figure 2.** Circular dichroism spectra at 3 °C of (A) native SLO-1 in 0.1 M MES, pD 7 (light solid line), and native SLO-1 in 0.1 M MES, pD 7, in saturated sucrose solution (dashed line) and the Gaussian sum (dark solid line) from simultaneous fits to the CD and MCD data (individual Gaussian contributions are dashed), (B) native SLO-1 + 50% (v/v) glycerol-$d_3$, and (C) native SLO-1 minus 60% (native SLO + 50% glycerol-$d_3$), renormalized. Native SLO-1 in sucrose data are only shown down to 7000 $cm^{-1}$ as the sucrose was not deuterated, producing a high noise level at lower energies.

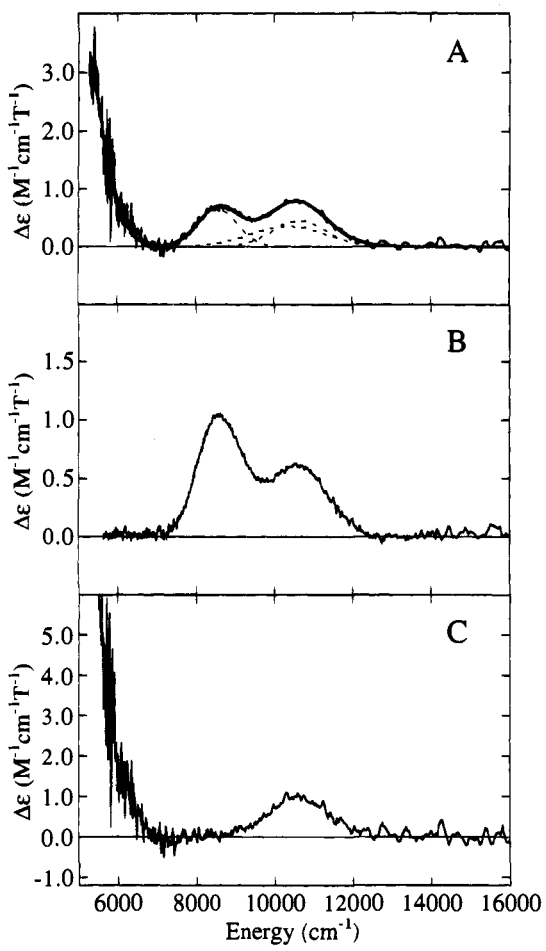


**Figure 3.** Magnetic circular dichroism spectra at 6 T and 4.2 K of (A) native SLO-1 in 0.1 M MES, pD 7, in saturated sucrose solution (light solid line) and the Gaussian sum (dark solid line) from simultaneous fits to the CD and MCD data (individual Gaussian contributions are dashed), (B) native SLO-1 + 50% (v/v) glycerol-$d_3$, and (C) native SLO-1 minus 60% (native SLO + 50% glycerol-$d_3$), renormalized.

ion $^5D$ ground state by an energy of $10Dq_{T_d} = -4/9(10Dq_{O_h})$, which will put the $^5E \rightarrow {}^5T_2$ spin-allowed transition at ~5000 $cm^{-1}$. These possible d-orbital splitting patterns of a ferrous center can be directly probed using CD and MCD spectroscopies in the NIR spectral region to determine the geometric environment of a ferrous site.

Figure 2A shows the 3 °C NIR CD spectrum of native SLO-1. There are positive features at <6000 and 10 700 $cm^{-1}$, as well as a small positive shoulder at ~8000 $cm^{-1}$ and weak negative intensity at 9200 $cm^{-1}$. Variation of the pD of the buffer solution from 5.6 to 11 produces no change in the NIR CD spectrum of native SLO-1, showing that the spectrum is not due to a pH-dependent mixture. Addition of glycerol to native SLO-1 produces the NIR CD spectra shown in Figure 2B. Gaussian resolution of the NIR CD spectra of SLO-1 in glycerol shows a positive band at 8600 $cm^{-1}$ and a negative feature at 10 300 $cm^{-1}$. Thus, the addition of glycerol to native SLO-1 produces a CD spectrum in the LF region consistent with a six-coordinate ferrous active site with distorted octahedral geometry. Glycerol is the usual glassing agent for low-temperature spectroscopy; however, since it perturbs the native SLO-1 active site, it is unsuitable for low-temperature spectroscopic studies of the native site. Sucrose was found to be a suitable glassing agent as addition to native SLO-1 causes no change in the NIR CD spectrum (Figure 2A, heavy dashed line).

The low-temperature NIR MCD spectrum of native SLO-1 in sucrose (Figure 3A) shows three positive peaks, at <5500, 9200, and 10 500 $cm^{-1}$. As no single ligand field geometry of a high-spin ferrous site can have more than two d → d transitions in the 4000−13000 $cm^{-1}$ region (*vide infra*), native SLO-1 in sucrose must exist as more than one form. The MCD spectrum of glycerol added to SLO-1 (Figure 3B) shows two positive bands at 8600 and 10 300 $cm^{-1}$, which are the same energies as in the native SLO-1 + glycerol CD spectrum (Figure 2B). Comparison of the MCD spectra in parts A and B of Figure 3 indicates the possibility that the six-coordinate species in Figure 3B is also contributing to the native SLO-1 spectra. Further examination of the native SLO-1 CD spectrum in Figure 2A shows the weak positive shoulder at ~8000 $cm^{-1}$ to be at the same energy as the positive intensity of the native SLO-1 + glycerol CD spectrum (Figure 2B). Also the band shape in Figure 2A from 9000 to 12 000 $cm^{-1}$ is indicative of a combination of negative and positive features with offset energies. Taken together, the CD and MCD data suggest that the same six-coordinate species in the glycerol-added form is a component in native SLO-1. Varying amounts of the six-coordinate SLO-1 + glycerol MCD signal (Figure 3B) were subtracted from the native SLO-1 MCD spectrum (Figure 3A). A two-peak difference spectrum was obtained if an amount corresponding to 60% of the SLO-1 + glycerol MCD signal was subtracted. Subtraction of any more or less than 60 ± 5% produced a three-peak difference spectrum in the MCD, which

is not appropriate for a single ferrous site. Subtraction of 60% of the native + glycerol signals and renormalization give the CD and MCD spectra of the second species present in the native enzyme, shown in Figures 2C and 3C, respectively. The NIR CD and MCD spectra of the second component present in native SLO-1 have two positive d → d bands at ~5000 and 10 600 $cm^{-1}$ ($\Delta^5E_g$ = ~5600 $cm^{-1}$), consistent with a five-coordinate square pyramidal ferrous site geometry. Simultaneous Gaussian fitting analyses of the native SLO-1 CD and MCD spectra confirm the presence of four bands (Figures 2A and 3A). The CD and MCD spectra of native SLO-1 have bands at ~5000 and 10 600 $cm^{-1}$ due to the five-coordinate component and bands at 8600 and 10 300 $cm^{-1}$ due to the six-coordinate component.

VTVH MCD can be used to probe the ground states of high-spin $Fe^{2+}$ active sites even in a mixture by focusing on an MCD band associated with a specific component of the mixture. MCD intensity for paramagnetic centers will increase with increasing field and decreasing temperature (*C*-terms).[51,52] However, at very low temperature and high magnetic field, this *C*-term intensity will saturate. This saturation magnetization behavior is observed by plotting the MCD intensity of a peak *vs* $\beta H/2kT$, which will show that the incremental increase in the MCD signal decreases with increasing magnetic field, eventually leveling off at high field. Saturation magnetization curves obtained at a series of fixed temperatures with variation in magnetic field plotted *vs* $\beta H/2kT$ will be nested,[53] *i.e.*, they will not superimpose, if the ground state has an integer spin, as in the case of high-spin $Fe^{2+}$ which has an $S = 2$ ground state. An $S = 2$ state will undergo zero (magnetic) field splitting (ZFS) due to the axial (*D*) and rhombic (*E*) components of the ligand field according to the spin Hamiltonian[54] in eq 1.

$$\mathscr{H} = D[(S_z)^2 - (1/3)S(S+1)] + E[(S_x)^2 + (S_y)^2] + g_{\parallel}\beta H_{\parallel} + g_{\perp}\beta H_{\perp} \quad (1)$$

The $M_S = \pm 2$ to $M_S = \pm 1$ sublevel axial splitting is $3D$ and the $M_S = \pm 1$ to $M_S = 0$ sublevel splitting is $D$, with the lowest sublevel being $M_S = 0$ if $D$ is positive or $M_S = \pm 2$ if $D$ is negative (Figure 1B). It is important to note that integer spin systems produce non-Kramers doublets which will split due to a nonzero rhombic ZFS (*i.e.*, $|E| \neq 0$ in eq 1) even in the absence of a magnetic field. When $D$ is negative, the $S = 2$ system can be modeled as an isolated $M_S = \pm 2$ non-Kramers doublet which is split by an amount $\delta$ (Figure 1B, right) due to the rhombic component of the ligand field. This also results in real wave functions $|X\rangle$ and $|Y\rangle$ which are equal mixtures of the MCD active $|+2\rangle$ and $|-2\rangle$ components.[16] These have an opposite MCD sign and cancel. When a magnetic field is applied, the $M_S = \pm 2$ sublevel splitting increases due to the Zeeman effect by a factor of $g_{\parallel}\beta H \cos\theta$ (where $\theta$ is the angle between the magnetic field and the molecular *z*-axis), and the wave functions change, becoming the pure complex, $|+2\rangle$ and $|-2\rangle$, and thus MCD active at higher fields.[16] MCD saturation magnetization data can be fit using an orientation-averaging function (eq 2) for the intensity of a non-Kramers doublet,[16] to quantitatively determine the ground-state parameters $g_{\parallel}$ and $\delta$ in Figure 1B, and an additional *B*-term contribution to intensity, which is due

$$\Delta\epsilon = A_{\text{satlim}} \int_0^{\pi/2} \frac{\cos^2\theta \sin\theta}{[\delta^2 + (g_{\parallel}\beta H \cos\theta)^2]^{1/2}} (g_{\parallel}\beta H) \tanh\left[\frac{[\delta^2 + (g_{\parallel}\beta H \cos\theta)^2]^{1/2}}{2kT}\right] d\theta + B_0 H \quad (2)$$

to field-induced mixing of higher energy states into the ground state.[22] In eq 2, which assumes pure *xy*-polarization, $A_{\text{satlim}}$ is the *C*-term intensity factor, $\beta$ is the Bohr magneton, $H$ is the magnetic field, $k$ is Boltzmann's constant, $T$ is the absolute temperature, and $B_0$ is the *B*-term contribution (reported as a percentage of $A_{\text{satlim}}$).

When $D$ is positive (Figure 1B, left), the $S = 2$ system can be modeled by three levels, $M_S = 0$ and $\pm 1$, as the $M_S = \pm 2$ levels are $3D$ higher in energy and do not influence the data over the normal temperature range for saturation magnetization experiments.[55] For a pure *xy*-polarized transition, the $M_S = 0$ ground level cannot contribute MCD intensity but the $M_S = \pm 1$ levels can, so the MCD intensity is zero at low temperature and increases as the $M_S = \pm 1$ levels become thermally populated. If some *z*-polarization is also present, the effects of the magnetic field along the *x* (and *y*) direction become important. This would mix the $M_S = 0$ in Figure 1B, left, with one component of the $M_S = \pm 1$. The $M_S = 0$ level and one partner of the $M_S = \pm 1$ level then behave like a non-Kramers doublet with a ZFS of $D$ $cm^{-1}$, and there remains a third Zeeman-inactive level at $D$ $cm^{-1}$. The MCD signal in this case is most intense at low temperature, like a *C*-term, and the lowest temperature data can be modeled by eq 2 with $\delta = D$, but deviates from eq 2 at higher temperatures when the Zeeman-inactive partner of the $M_S = \pm 1$ level becomes thermally populated.[56] In general, VTVH data of $+D$ systems will be more nested than data of $-D$ systems since the ZFS is on the order of $D$, not $\delta$ from Figure 1B.

To investigate the ground-state properties of the two forms of native SLO-1, VTVH MCD data for a series of different temperatures were taken for the bands associated with the pure six- and five-coordinate sites. Figure 4A shows the saturation magnetization data plotted *vs* $\beta H/2kT$ for the 5800 $cm^{-1}$ (five-coordinate) band of the native form of SLO-1 from Figure 3A, and Figure 4B shows the VTVH MCD data for the 8600 $cm^{-1}$ band of SLO-1 + glycerol from Figure 3B (the 8600 $cm^{-1}$ (six-coordinate) data for SLO-1 in sucrose are nearly identical). The curves for both are nested, consistent with the integer spin $S = 2$ ground states. The MCD data were fit with eq 2, and Table 1 shows the corresponding experimentally determined ground-state parameters. Fitting the VTVH MCD data for the five-coordinate site to the $-D$ model (Figure 1B, right) yields $\delta = 7 \pm 1$ $cm^{-1}$ and $g_{\parallel} = 9 \pm 2$, which would correspond to the spin Hamiltonian parameters of $D = -21 \pm 3$ $cm^{-1}$ and $|E/D| \approx 0.33$.[57] This is a large value for $D$,[55] so the $+D$ model was also considered. Fitting a $+D$, three-level model (Figure 1B, left) to these data gives energy levels at 0, 7, and 15 $cm^{-1}$ (Figure 4A, lines), which correspond to the spin Hamiltonian values of $D \approx +10$ $cm^{-1}$ and $|E/D| \approx 0.1$. If the $-D$ model is applied to the six-coordinate site of SLO-1 in glycerol, the values of $\delta = 10$ $cm^{-1}$ and $g = 10.5$ are obtained. Both of these values are out of the expected range,[16,55] indicating that a $+D$ model

(51) Buckingham, A. D.; Stephens, P. J. *Annu. Rev. Phys. Chem.* **1966**, *17*, 399.

(52) Piepho, S. B.; Schatz, P. N. *Group Theory in Spectroscopy With Applications to Magnetic Circular Dichroism*; John Wiley and Sons: New York, 1983.

(53) Thomson, A. J.; Johnson, M. K. *Biochem. J.* **1980**, *191*, 411.

(54) Abragam, A.; Bleaney, B. *Electron Paramagnetic Resonance of Transition Ions*; Dover Publications, Inc.: New York, 1986.

(55) Solomon, E. I.; Pavel, E. G.; Loeb, K. E.; Campochiaro, C. *Coord. Chem. Rev.*, in press.

(56) If $|E| \neq 0$, the $M_S = \pm 1$ doublet will split by $6|E|$, and if *yz*-polarization is present, the lower energy partner of the doublet will interact with the $M_S = 0$ level for $H$ along the molecular *x*-axis. Conversely, if *xz*-polarization is present, the higher energy partner of the $M_S = \pm 1$ doublet will interact with the $M_S = 0$ level for $H$ along the molecular *y*-axis.

(57) Note that *z*-polarization contributions were considered for all the systems presented in this paper and were not found to substantially improve the fits.

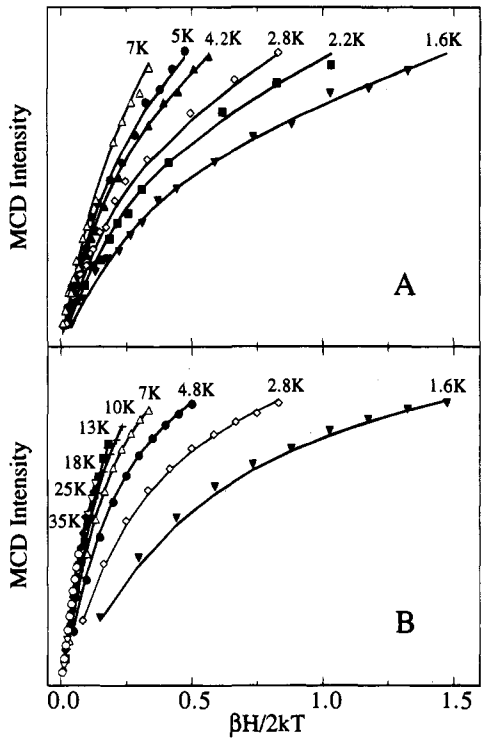


**Figure 4.** Saturation magnetization curves of the MCD amplitude plotted as a function of $\beta H/2kT$ for (A) native SLO-1 in sucrose obtained for the 5800 $cm^{-1}$ band in Figure 3A and (B) SLO-1 in glycerol obtained for the 8600 $cm^{-1}$ band in Figure 3B. The symbols show the raw data, and the solid lines are the fits to the data using the parameters in Table 1. The SLO-1 in glycerol parameters also fit the saturation magnetization data for the 8600 $cm^{-1}$ band in SLO-1 in sucrose.

**Table 1.** Experimental d-Orbital Splittings and Ligand Field Parameters

| parameter[a] | 5C SLO-1 (5800 $cm^{-1}$) | 6C SLO-1 (8600 $cm^{-1}$) | 15-RLO (8600 $cm^{-1}$) | 15-HLO (8600 $cm^{-1}$) |
|---|---|---|---|---|
| $\Delta^5E_g$ ($cm^{-1}$) | 5600 | 1700 | 1650 | 2000 |
| $g_{\|\|}$ | 9 | 10.5 | 9.0 | ~9 |
| $\delta$ ($cm^{-1}$) | 7 | 9.6 | 4.4 | ~4 |
| *B*-term (% of *C*-term) | 4 | 1.5 | 2.5 | ~2.5% |
| $\Delta$ ($cm^{-1}$) | $+700 \pm 200$ | $+450 \pm 200$ | $-500 \pm 200$ | $-500 \pm 200$ |
| $\|V\|$ ($cm^{-1}$) | $270 \pm 150$ | $150 \pm 110$ | $270 \pm 160$ | $270 \pm 160$ |
| $\|V/2\Delta\|$ | $0.19 \pm 0.05$ | $0.16 \pm 0.05$ | $0.27 \pm 0.05$ | $0.27 \pm 0.05$ |

[a] See Figure 1 for parameter definitions.

must also be applied to this system. A $+D$ fit gives an energy level spacing of 0, 10, and 18 $cm^{-1}$, corresponding to $D = +13$ $cm^{-1}$ and $E/D = 0.1$, which are well within the range expected for $+D$ values. This fit is shown in Figure 4B, lines, and also describes the SLO-1 in sucrose VTVH MCD data, confirming that these two sites are very similar. These results indicate that glycerol (and other alcohols) does not directly bind to the ferrous site but rather causes a conformational change near the active site, shifting the five-coordinate component to six-coordination.

The ground-state parameters obtained from fitting VTVH MCD data can be related to the splittings of the orbital components $\Delta$ and $V$ of the $^5T_{2g}$ ground state shown in Figure 1A.[16,55,58] Axial distortion of an octahedral complex splits the $^5T_{2g}$ ground state into $^5E$ and $^5B_2$ states, $^5E$ being lowest in energy in the weak-axial case which corresponds to weak-field axial ligands, tetragonal elongation, or some square pyramidal geometries. This splitting is defined as $-\Delta$ for $^5E$ lowest in energy. The $^5E$ state will further split into two orbitally nondegenerate components with a rhombic distortion by an amount $V$ (see Figure 1A). From Figure 1A, all ground states are $S = 2$, and these become zero field split due to spin–orbit coupling over all the components of the $^5T_{2g}$ state. Thus, the spin Hamiltonian parameters, $\delta$ and $g_{\|}$ for negative ZFS and $D$ and $E$ for positive ZFS, can be related to $\Delta$ and $V$ to obtain the orbital splittings of the $^5T_{2g}$ state, which directly correlate with the $t_{2g}$ orbital splittings. This methodology has been presented in detail elsewhere,[16,55,58] and the results for both the five- and six-coordinate forms are summarized in Table 1. The five-coordinate site (5800 $cm^{-1}$ band) has a $\Delta = +700$ $cm^{-1}$ while the six-coordinate site (8600 $cm^{-1}$ band) has a $\Delta = +450$ $cm^{-1}$. This is consistent with the five-coordinate site having a greater ligand field distortion than the six-coordinate site, and hence greater $t_{2g}$ orbital splittings.

We have attempted to approach the different crystallization conditions used by the two SLO-1 crystal structure studies to see the effects on the NIR CD/MCD data of the native SLO-1 active site. Boyington *et al.*[6] used 4.6 M sodium formate, 1.0 M ammonium acetate, and 600 mM lithium chloride in 20 mM MES buffer, pH 7. SLO-1 was prepared in 20 mM MES buffer, pD 7; addition of 1 M sodium formate, 0.7 M ammonium acetate, and 600 mM lithium chloride caused no change in the native SLO-1 NIR CD spectrum in Figure 2A; any higher concentrations of these salts caused precipitation of the protein. Thus, the buffering conditions and the addition of high concentrations of the salts used to precipitate the SLO-1 cause no change in the active site of native ferrous SLO-1. Minor *et al.*[11] used 0.2 M sodium acetate buffer, pH 5.6, containing 8% (w/v) polyethylene glycol (PEG)-3400. SLO-1 in 0.2 M sodium acetate buffer, pD 5.6, has an NIR CD spectrum identical to that of native SLO-1 in sulfonic acid buffers. Addition of any amount of PEG-3400, -1000, or -400 to samples with protein concentrations necessary for NIR CD spectroscopy (0.5–2 mM) caused immediate precipitation. Therefore, the pH and buffer used in the Minor *et al.*, crystallization also cause no change in the native SLO-1 active site; however, the effect of PEG could not be determined.

As the addition of alcohols has been shown to alter the EPR spectra of $Fe^{3+}$ SLO-1,[59,60] the effects of alcohols on native $Fe^{2+}$ SLO-1 were investigated by NIR CD spectroscopy. The CD spectra of SLO-1 + 750 mM ethanol and SLO-1 in 50% ethylene glycol have the same band shape and intensity as the CD spectrum of SLO-1 in glycerol (Figure 2B). Thus, three different alcohols have the same effect of shifting the five- and six-coordinate mixture of native SLO-1 to the pure six-coordinate form. The anaerobic addition of substrate to native SLO-1 was also investigated. The NIR CD spectrum of SLO-1 with 12-fold excess of sodium linoleate is identical to that of native SLO-1 + alcohols, indicating that substrate binding shifts the native enzyme to the pure six-coordinate form and also that the alcohols appear to interact with the substrate binding site and not directly with the iron. The addition of up to 500-fold molar excess of $NaN_3$ to native SLO-1 causes no change relative to the native SLO-1 NIR CD spectrum. Anaerobic addition of a 500-fold molar excess of $NaN_3$ to SLO-1 + 12-fold linoleate again causes no change in the NIR CD spectrum. Thus, in contrast with our results on metapyrocatechase,[61] which also has a stable $Fe^{2+}$ active site in air but is activated by substrate binding, linoleate substrate binding does not appear to activate the ferrous SLO-1 site for small molecule binding. Substrate

(58) Solomon, E. I.; Zhang, Y. *Acc. Chem. Res.* **1992**, *25*, 343.
(59) Gaffney, B. J.; Mavrophilipos, D. V.; Doctor, K. S. *Biophys. J.* **1993**, *64*, 773.
(60) Slappendel, S.; Aasa, R.; Malmström, B. G.; Verhagen, J.; Veldink, G. A.; Vliegenthart, J. F. G. *Biochim. Biophys. Acta* **1982**, *708*, 259.
(61) Mabrouk, P. A.; Orville, A. M.; Lipscomb, J. D.; Solomon, E. I. *J. Am. Chem. Soc.* **1991**, *113*, 4053.

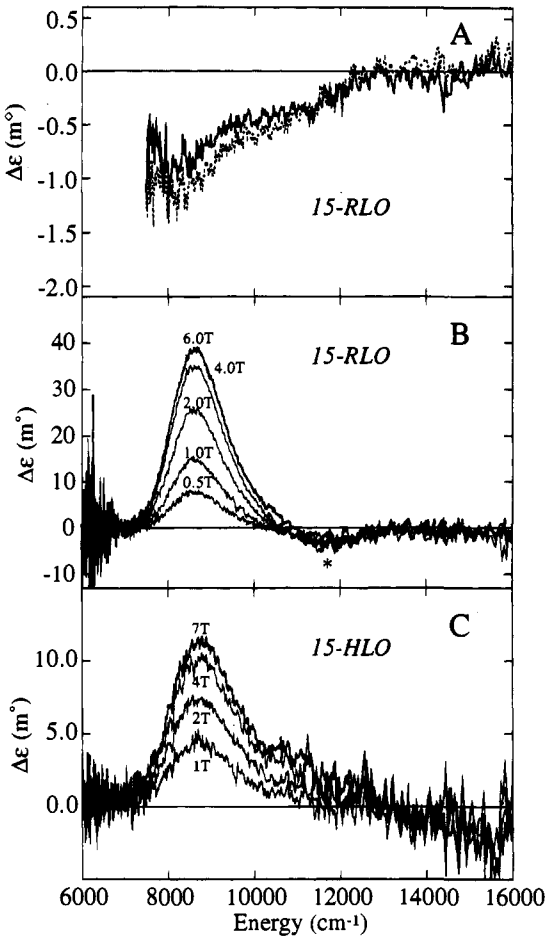


**Figure 5.** (A) CD spectra at 3 °C of 0.40 mM native 15-RLO in 20 mM sodium phosphate, pH 7.0, and 0.1 M NaCl (solid line) and in the presence of ~30% (v/v) glycerol-$d_3$ (dashed line). (B) MCD spectra at 4.2 K of 0.9 mM native 15-RLO in 20 mM sodium phosphate, pD 7, and 0.1 M NaCl + 50% (v/v) glycerol-$d_3$. (C) MCD spectra at 4.2 K of 0.5 mM native 15-HLO in 20 mM sodium phosphate, pD 7, and 0.1 M NaCl + 50% (v/v) glycerol-$d_3$. The magnitudes of the applied magnetic field are indicated. Native 15-RLO CD data are only shown down to 7000 $cm^{-1}$ as the buffer used was not deuterated due to protein instability. The asterisk indicates a <2% heme impurity.

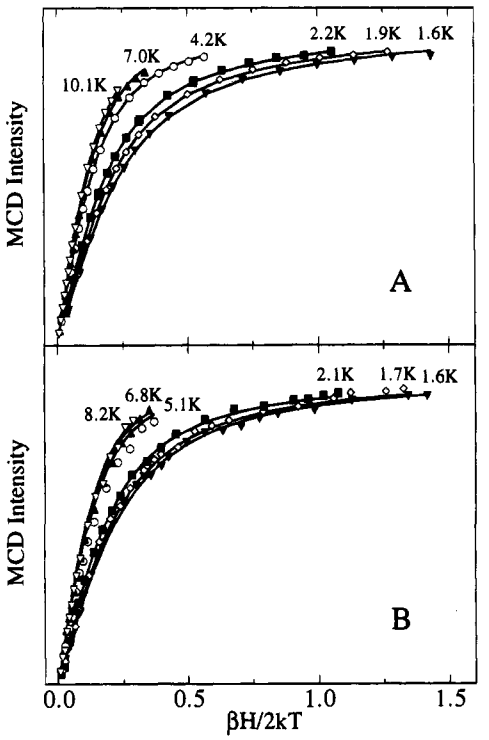


**Figure 6.** Saturation magnetization curves of the MCD amplitude plotted as a function of $\beta H/2kT$ for (A) native 15-RLO under the conditions of Figure 5B for the 8600 $cm^{-1}$ band and (B) native 15-HLO under the conditions of Figure 5C for the 8600 $cm^{-1}$ band. The symbols show the raw data, and the solid lines are the fits to the data using the parameters in Table 1.

binding does cause the mixture of forms of native SLO-1 to convert to purely six-coordinate, indicating that the six-coordinate component of native SLO-1 may be related to the catalytically relevant form.

**NIR CD/MCD of 15-RLO and 15-HLO.** The NIR CD spectrum of native 15-RLO (Figure 5A, solid line) shows two negative features at ~8500 and ~10 500 $cm^{-1}$. Addition of glycerol to native 15-RLO gives the same spectrum (Figure 5A, dashed line) as native 15-RLO. Therefore, unlike native SLO-1, the active site of native 15-RLO is not perturbed by glycerol, so glycerol is a suitable glassing agent for low-temperature MCD studies. Figure 5B shows the 4.2 K NIR MCD spectrum of native 15-RLO in glycerol. Additionally, the 4.2 K MCD spectrum of 15-RLO in sucrose was obtained and shows no change relative to 15-RLO in glycerol. Both the 15-RLO in glycerol and in sucrose spectra exhibit an asymmetric band peaking at 8650 $cm^{-1}$ with a shoulder at ~10 300 $cm^{-1}$. The two bands at ~10 000 $cm^{-1}$ split by ~2000 $cm^{-1}$ are indicative of a six-coordinate ferrous site (*vide supra*). Thus, in contrast to native SLO-1, native 15-RLO exists as a pure six-coordinate form. As with native 15-RLO, the native 15-HLO NIR CD spectral features are weak and show no change upon addition of glycerol. The NIR MCD spectrum of native 15-HLO in glycerol (Figure 5C) shows two features at 8750 and ~10 750 $cm^{-1}$, indicative of a six-coordinate ferrous active site. Thus, the two native mammalian 15-LOs have similar CD and MCD spectra and thus $\Delta^5E_g$ excited-state splittings and must both exist as pure six-coordinate forms.

Saturation magnetization data were also obtained for the two mammalian 15-LOs. Parts A and B of Figure 6 show the MCD intensity *vs* $\beta H/2kT$ for 15-RLO and 15-HLO, respectively, both taken at 8600 $cm^{-1}$. The curves are nested, indicative of an integer spin $S = 2$ ground state, and also saturate with increasing field, reaching a limiting intensity at high field. They behave similarly to each other, but are strikingly different from the saturation magnetization curves for the six-coordinate SLO-1 site (Figure 4B). The MCD data were fit (Figure 6, solid lines) with eq 2 to determine the ground-state parameters $g_{||}$ and $\delta$ and the *B*-term contribution to intensity (Table 1). Both the 15-RLO and 15-HLO VTVH MCD data sets were fit with a value of $\delta$ of 4.4 $cm^{-1}$, which is small relative to both the five- and six-coordinate forms of SLO-1 (7 and 9.6 $cm^{-1}$). The data were well described by the $-D$ model (Figure 1B, right), and when a $+D$ (Figure 1B, left) fit was attempted, the energy of the third level floated above the experimental range, further supporting the $-D$ analysis. Applying the developed methodology,[16,55,58] the values $\Delta = -500$ $cm^{-1}$ and $V = 270$ $cm^{-1}$ were obtained for both 15-RLO and 15-HLO, which are comparable in magnitude to the value of $\Delta = +450$ $cm^{-1}$ obtained for the six-coordinate form of SLO-1, but the sign is changed. Figure 7 summarizes these experimentally determined d-orbital splittings (Figure 1A) for the two native SLO-1 forms, (A) five-coordinate and (B) six-coordinate, and for (C) 15-RLO and (D) 15-HLO.

**XAS of SLO-1, 15-RLO, and 15-HLO in Glycerol.** Fe K-edge X-ray absorption spectra of ferrous SLO-1, 15-RLO, and 15-HLO have been compared to spectra of four-, five-, and six-coordinate ferrous model complexes to obtain an additional

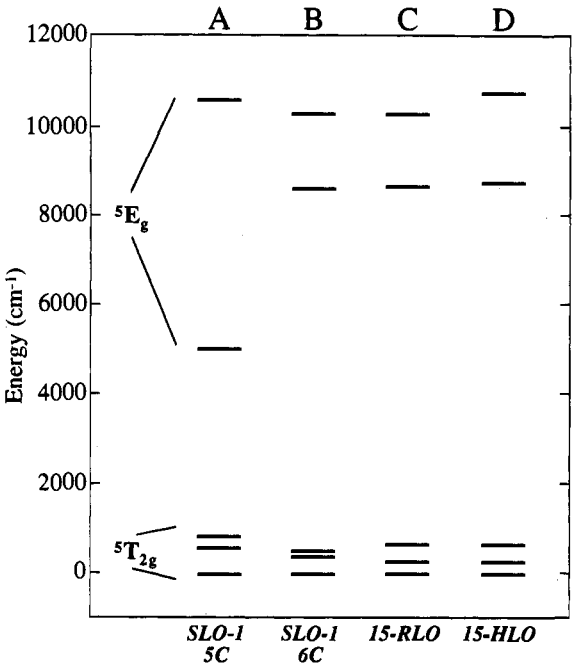


**Figure 7.** Experimentally determined d-orbital energy level diagrams using the results in Table 1 for (A) five-coordinate SLO-1, (B) six-coordinate SLO-1, (C) 15-RLO, and (D) 15-HLO.

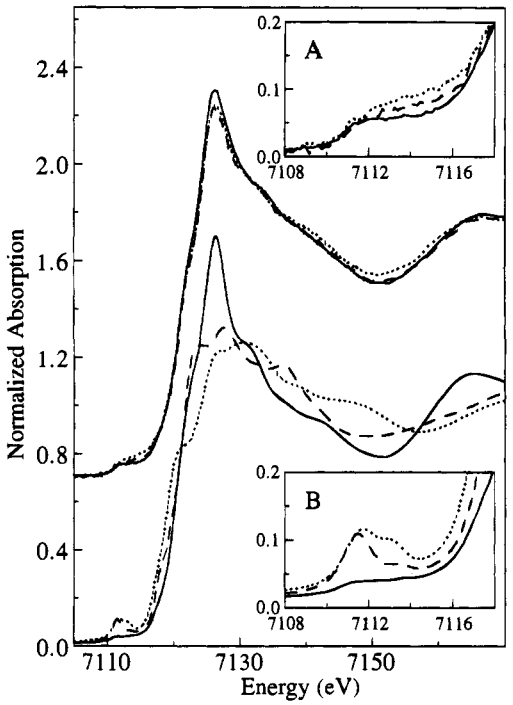


**Figure 8.** Fe K XAS edge spectra (offset by +0.7) of SLO-1 (solid line), 15-RLO (dashed line), and 15-HLO (dotted line) (upper portion, where inset A shows an expansion of the 1s → 3d pre-edge region). The lower portion shows the Fe K XAS edge spectra of four-, five- and six-coordinate ferrous model complexes Fe(HB(3,5-*i*Pr$_2$pz)$_3$)Cl (dotted line), [Fe(trpn)(MeCN)](CF$_3$SO$_3$)$_2$ (dashed line), and [Fe(imidazole)$_6$]Cl$_2$ (solid line). Inset B is an expansion of the 1s → 3d pre-edge region for the model complexes.

determination of the coordination number of the iron active site in the LOs. All three protein samples contained glycerol to ensure that a pure form was being studied (*vide supra*). The XAS edge spectra for SLO-1, 15-RLO, and 15-HLO are shown in the upper portion of Figure 8, while the lower portion contains spectra of representative four-, five-, and six-coordinate ferrous model complexes: Fe(HB(3,5-*i*Pr$_2$pz)$_3$)Cl,[26] [Fe(trpn)(MeCN)](CF$_3$SO$_3$)$_2$,[27] and [Fe(imidazole)$_6$]Cl$_2$.[29] The lowest energy peaks arise from the weak 1s → 3d transition which is at ~7112 eV followed by the 1s → 4p transition at ~7125 eV. An expanded view of the 1s → 3d pre-edge region is shown for the three LOs as well as for the model complexes in Figure 8, insets A and B, respectively. The energies and areas of the pre-edge features were determined by fits to the data and are presented in Table 2. The SLO-1, 15-RLO, and 15-HLO spectra all have a very broad low-intensity pre-edge feature which can be fit with two features that have a total pre-edge area of ~0.08. Fe(HB(3,5-*i*Pr$_2$pz)$_3$)Cl, [Fe(trpn)(MeCN)](CF$_3$SO$_3$)$_2$, and [Fe(imidazole)$_6$]Cl$_2$ all have two pre-edge features split by ~2 eV with varying intensities. The four-coordinate complex has the most intense pre-edge feature (0.188 total area), while the six-coordinate complex has the least intense pre-edge feature (0.032). The "white line", attributed to the 1s → 4p transition at ~7125 eV, is very similar in shape and intensity in all three LO samples, while this feature differs drastically in shape between the four-, five-, and six-coordinate ferrous complexes (Figure 8).

**Table 2.** Ferrous Model Complex and LO Pre-edge Energies and Areas

| sample | CN[a] | pre-edge energy (eV) | pre-edge area[b] |
|---|---|---|---|
| Fe(HB(3,5-*i*Pr$_2$pz)$_3$)Cl | 4 | 7111.6, 7113.2 | 0.188 ± 0.005 |
| [Fe(trpn)(MeCN)](CF$_3$SO$_3$)$_2$ | 5 | 7111.5, 7113.4 | 0.152 ± 0.007 |
| [Fe(imidazole)$_6$]Cl$_2$ | 6 | 7111.3, 7113.6 | 0.032 ± 0.002 |
| SLO-1 in glycerol | | 7111.5, 7113.1 | 0.084 ± 0.011 |
| 15-RLO | | 7111.8, 7113.1 | 0.082 ± 0.025 |
| 15-HLO | | 7111.7, 7113.3 | 0.084 ± 0.015 |

[a] CN = coordination number. [b] Pre-edge areas and errors were determined from fits to the data. See the Experimental Section for a discussion of the fitting procedure and error determination.

The 1s → 3d pre-edge feature can be used to probe the coordination number of the iron in the active site of the LOs. The 1s → 3d transition is formally electric dipole forbidden, but gains intensity through an allowed quadrupole transition and more dominantly by 4p mixing into the 3d states as a result of the noncentrosymmetric environment of the metal site. It has been shown for ferric complexes that when the symmetry of the iron site is lowered, the pre-edge intensity increases due to an increase in the 3d−4p mixing.[62] In the high-spin ferrous case, two final states of maximum spin multiplicity can be reached, $^4$F and $^4$P. The free ion splitting of the $^4$F and $^4$P is 2 eV[63] and is readily resolvable at the Fe K-edge. The splitting of the pre-edge in Fe(HB(3,5-*i*Pr$_2$pz)$_3$)Cl, [Fe(trpn)(MeCN)](CF$_3$SO$_3$)$_2$, and [Fe(imidazole)$_6$]Cl$_2$ is attributed to this $^4$F and $^4$P splitting of approximately 2 eV. As in the ferric case, the pre-edge area of the ferrous four-coordinate complex is greater than that of the five-coordinate complex, which is greater than that of the six-coordinate complex (Figure 8, inset B). However, the ferrous case is more complicated since there are two pre-edge features which can have different intensity distributions. We are currently investigating the variation of this intensity distribution in a number of ferrous complexes.[64] Empirically the pre-edge features of SLO-1, 15-RLO, and 15-HLO look much more similar in shape and intensity to that of the six-coordinate ferrous model and quite different from those of the four- and five-coordinate models. The fitted area of the pre-edge features of the LOs at ~0.08 is higher than that of [Fe-

(62) Roe, A. L.; Schneider, D. J.; Mayer, R. J.; Pyrz, J. W.; Widom, J.; Que, L., Jr. *J. Am. Chem. Soc.* **1984**, *106*, 1676.
(63) Shulman, R. G.; Yafet, Y.; Eisenberger, P.; Blumberg, W. E. *Proc. Natl. Acad. Sci. U.S.A.* **1976**, *73*, 1384.
(64) Westre, T. E.; Hedman, B.; Hodgson, K. O.; Solomon, E. I. To be published.

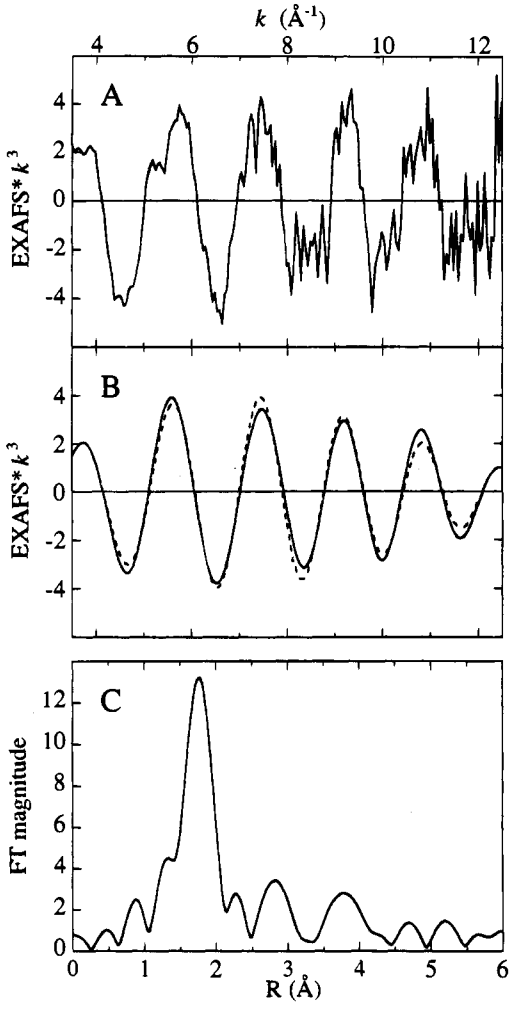


**Figure 9.** (A) EXAFS data ($\times k^3$) for SLO-1 in glycerol. (B) Fit to the Fourier filtered data. The solid line represents the data (FT back-transform range 1.0−2.25 Å) while the dashed line is the fit to the data with one shell of N (Table 3, fit 6). (C) Fourier transform (non-phase-shift-corrected) over the $k$ range 3.5−12.5 Å$^{-1}$ of the EXAFS data of SLO-1.

(imidazole)$_6$]Cl$_2$ at 0.03. The larger pre-edge in the LOs can be attributed to an overall less symmetric iron site caused by mixed ligation and variation in bond lengths. However, the shape of the LOs' pre-edge feature is very similar to that of [Fe(imidazole)$_6$]Cl$_2$ and other six-coordinate ferrous complexes.[64] In addition, the shapes of the "white line" in the SLO-1, 15-RLO, and 15-HLO spectra at ~7127 eV are very much alike and similar to that in the six-coordinate [Fe(imidazole)$_6$]-Cl$_2$ spectrum. These results are consistent in indicating that all three LOs in glycerol have a six-coordinate iron active site. Thus, the XAS edge results corroborate the MCD results described earlier.

EXAFS studies of SLO-1 in glycerol were also pursued to obtain metrical information on the iron active site of the pure six-coordinate form (*vide supra*). High-quality, high-$k$ EXAFS data could not be obtained on the 15-HLO or 15-RLO samples due to the low protein concentration of ~1 mM. The EXAFS spectrum of SLO-1 in glycerol is shown in Figure 9A, and the Fourier transform (FT), taken over the $k$ range of 3.5−12.5 Å$^{-1}$, is shown in Figure 9C. Curve-fitting was performed on filtered first-shell contributions over the $k$ range 4−12 Å$^{-1}$. Fits were performed by stepping through fixed coordination numbers while allowing the bond distance and $c2$ to vary. $c2$ is the amplitude parameter which has the functional form of the Debye−Waller factor, *i.e.*, $\exp(xk^2)$, where $x = c2$ or $x = -2\sigma_{as}^2$.[23,30-32] As determined in these fits, the value of $c2$ is correlated to $\sigma_{as}^2$ only in a relative manner. Since $\Delta c2 = -2\Delta\sigma_{as}^2$, a more negative value of $c2$ denotes a larger value of $\sigma_{as}^2$ and thus a weaker bond or a greater distribution of distances for scatterers. The values of $c2$ for Fe−O from Fe(acetylacetonate)$_3$ and Fe−N from [Fe(1,10-phenanthroline)$_3$](ClO$_4$)$_3$ were −0.023 91 and −0.020 83, respectively. These values correspond to a well-ordered shell of nearest neighbors.

**Table 3.** Summary of EXAFS Curve-Fitting Results for SLO-1 in Glycerol[a]

| fit no. | element | CN[b] (fixed) | distance[c] | $c2$[d] | $F$ |
|---|---|---|---|---|---|
| 1 | O | 4 | 2.15 | −0.024 49 | 0.32 |
| 2 | O | 5 | 2.15 | −0.028 14 | 0.47 |
| 3 | O | 6 | 2.15 | −0.031 58 | 0.63 |
| 4 | N | 4 | 2.18 | −0.019 73 | 0.45 |
| 5 | N | 5 | 2.18 | −0.022 50 | 0.34 |
| 6 | N | 6 | 2.18 | −0.025 00 | 0.32 |
| 7 | O | 1 | 2.15 | −0.056 71 | 0.28 |
| | N | 5 | 2.18 | −0.022 99 | |
| 8 | O | 2 | 2.15 | −0.051 48 | 0.25 |
| | N | 4 | 2.18 | −0.020 86 | |
| 9 | O | 3 | 2.15 | −0.048 11 | 0.22 |
| | N | 3 | 2.18 | −0.018 30 | |
| 10 | O | 1 | 1.95[e] | −0.695 47 | 0.34 |
| | N | 5 | 2.18 | −0.022 50 | |
| 11 | O | 2 | 1.95[e] | −0.649 71 | 0.45 |
| | N | 4 | 2.18 | −0.019 73 | |
| 12 | O | 3 | 1.95[e] | −0.659 84 | 0.63 |
| | N | 3 | 2.18 | −0.016 50 | |
| 13 | O | 2 | 2.00[e] | −0.682 07 | 0.45 |
| | N | 4 | 2.18 | −0.019 73 | |
| 14 | O | 2 | 2.05[e] | −0.072 32 | 0.42 |
| | N | 4 | 2.18 | −0.019 78 | |
| 15 | O | 2 | 2.10[e] | −0.049 90 | 0.30 |
| | N | 4 | 2.18 | −0.020 53 | |

[a] FT range 3.5−12.5 Å$^{-1}$; FT back-transform range 1.0−2.25 Å. [b] CN = coordination number. [c] Errors in distances (±0.02 Å) are estimated from the variance between EXAFS fitting results and values from models of crystallographically known structure.[30] [d] $c2$ values for Fe−O from Fe(acetylacetonate)$_3$ and Fe−N from [Fe(1,10-phenanthroline)$_3$](ClO$_4$)$_3$ were −0.023 91 and −0.020 83, respectively. [e] Values fixed.

The FT peak centered at ~1.8 Å (non-phase-shift-corrected) could be adequately fit with either one shell of O's or N's (fits 1−6 in Table 3; Figure 9B) with average first-shell distances of 2.15 and 2.18 Å, respectively. Fits 1−3 with all O ligation matched the data better in the lower $k$ region, while fits 4−6 with all N ligation matched the data better in the higher $k$ region. The coordination number and $c2$ are highly correlated, as can be seen in fits 1−3 and 4−6 in Table 3, with the $c2$ values becoming more negative as the coordination number is increased. The $F$ value is lowest with a coordination number of 4 using the Fe−O parameters (fit 1) and a coordination number of 5 or 6 using the Fe−N parameters (fit 6, Figure 9B). Two-shell fits with both an O and a N contribution were also attempted (fits 7−9). These fits gave no indication that the first shell has two components since the distances remained the same (and thus not separable), the $c2$ parameters were highly correlated, and the $c2$ parameter of O increased to such a level where its resulting contribution was negligible. Previous results on SLO-1 in frozen buffered solution[14] indicated that there were two O's at a distance of 1.94 Å. Therefore, the possibility of a shorter low $Z$ contribution was further examined by fixing an Fe−O distance at 1.95, 2.00, 2.05, and 2.10 Å (fits 10−15) and letting both $c2$ values and the second-shell distance vary. When both distances of these two-shell fits were allowed to vary, the same results as in fits 7−9 were obtained. These fits to the data on SLO-1 in glycerol do not support a shorter Fe−O distance. The fit became significantly worse with the addition

of a second shell in that the $c2$ value for the shorter Fe−O contribution was more than an order a magnitude more negative than is chemically reasonable.

Fits were also performed where $c2$ was fixed at −0.023 91 and −0.020 83 for the Fe−O and Fe−N contributions, respectively, letting both the distance and coordination number vary. As expected, this gave the same results. The coordination numbers obtained from these fits were low, 3.8 for a fit with one O shell and 4.6 for a fit with one N shell. The low coordination numbers from these fits and the fact that the $c2$ values (when CN = 6) are more negative than the respective values for Fe(acetylacetonate)$_3$ and [Fe(1,10-phenanthroline)$_3$]-$(ClO_4)_3$ indicate that SLO-1 has a greater distribution of scatterers than the model complexes, as would be expected for the active site of a protein. We have observed experimentally that for a spread in first-shell distances of 0.15 Å for a six-coordinate complex with mixed O and N ligation, the $c2$ values were −0.034 08 for a fit with one shell of O and −0.028 16 for a fit with one shell of N. The fact that fits 3 and 6 have less negative $c2$ values, respectively, suggests that the spread of first-shell distances in SLO-1 is less than 0.15 Å. This is also supported by the fact that a two-shell fit (fits 7−9) does not match the data significantly better than a one-shell fit (fits 1−6) and that two shells should be readily discernible over the $k$-range 4−12 Å$^{-1}$ if the spread of first-shell distances is greater than ~0.1 Å.

In summary, the Fe K-edge shape and pre-edge intensity for all three 15-LO active sites are very similar to each other and all consistent with six-coordination. The EXAFS data of SLO-1 show that the iron active site has 5 ± 1 O/N ligands at ~2.16 Å.[65] The average bond length also supports a six-coordinate site: crystallographic information on ferrous model complexes with oxygen and nitrogen ligation gives average bond lengths of 2.16 ± 0.03 Å for six-coordinate sites,[66-70] 2.12 ± 0.01 Å for five-coordinate sites,[26,27] and 2.00 ± 0.01 Å for four-coordinate sites.[26] There is no indication of the previously reported shorter Fe−O distance.[14] Furthermore, our results show an average first-shell distance that is ~0.1 Å longer than the previous result of 2.05 Å.[14]

## Discussion

NIR CD and MCD spectroscopies allow the direct determination of the splitting of the ferrous $^5E_g$ excited state (see Figure 1A) which through LF theory is dependent on the coordination geometry.[55,58] Through analysis of the NIR CD and MCD spectra, it has been determined that native SLO-1 in solution exists as a nearly equal mixture of five- and six-coordinate forms. The two crystal structures[6,11] of SLO-1 have four common ligands, three histidines and the carboxylate terminus isoleucine. Our spectroscopic results indicate that one and two additional ligands are present in the five- and six-coordinate forms, respectively. One ligand is likely a water or hydroxide. Minor *et al.* leave this open as a possibility in their structure, while Boyington *et al.* find no evidence for a water-based ligand. Nelson[13] has performed an EPR line broadening experiment on $Fe^{3+}$ SLO-1 in $H_2{}^{17}O$ which showed evidence that in the ferric enzyme a water or hydroxide is present. The differing crystallization conditions do not appear to have an effect on the five- and six-coordinate active site mixture of SLO-1 in solution by NIR CD. Crystal packing interactions and the effects of PEG and higher concentrations of salts used in the Minor *et al.* and Boyington *et al.* crystallizations, respectively, can only be addressed through spectroscopic studies directly on the crystalline forms.

A significant difference in the crystal structures is in the binding of Asn$_{694}$. Minor *et al.* have this residue bound through the carbonyl oxygen of the amide side chain, while the side chain is 3.3 Å from the $Fe^{2+}$ in the Boyington *et al.* structure. An amide carbonyl oxygen would be a relatively weak ligand which could be perturbed by hydrogen bonding or steric effects. Boyington *et al.* have the asparagine side chain hydrogen bonded to a neighboring glycine. The asparagine is also conserved in all sequenced LOs, except rabbit reticulocyte and human 15-LOs. It is reasonable for the sixth ligand in the native six-coordinate SLO-1 site to be this asparagine. Structures A and B shown in Figure 10 are spectroscopically effective active site models built upon the crystallography[6,11] for the five- and six-coordinate SLO-1 forms. Since the ligands perturb the d-orbital energy levels in a way dependent on their arrangement around the ferrous center,[21,71] LF calculations[71] were performed on the two proposed SLO-1 structures (Figure 10A,B) as well as on

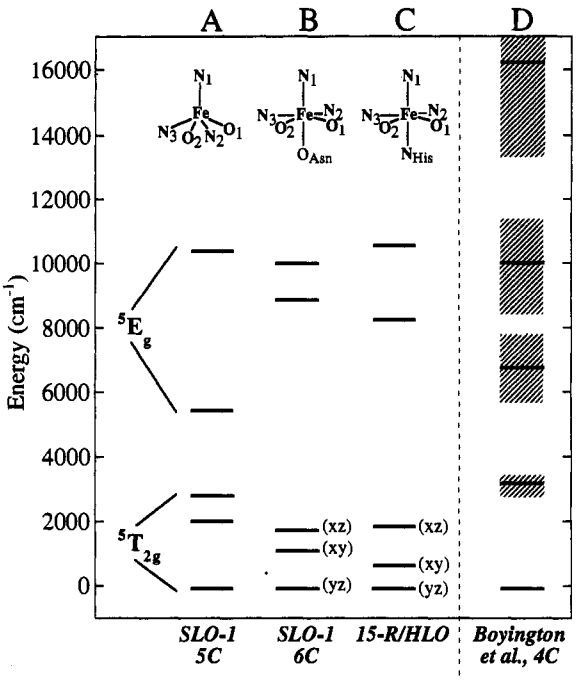


**Figure 10.** Theoretical LF energy level diagrams calculated for the spectroscopically effective structures of (A) the five-coordinate SLO-1 site, (B) the six-coordinate SLO-1 site, (C) the six-coordinate 15-R/HLO site, and (D) the four-coordinate crystallographically determined structure for SLO-1 by Boyington *et al.*[6] (D) includes a spread of energies associated with a reasonable range of $\alpha_2$ and $\alpha_4$ values. The orbital labels represent the primary component of the mixed wave functions resulting from the calculations. Ligand arrangements are based on the crystal structures in refs 6 and 11, where $N_1$ = N(His$_{504}$), $N_2$ = N(His$_{690}$), $N_3$ = N(His$_{499}$), $O_1$ = O(Ile$_{839}$), $O_2$ = O(H$_{(2)}$O), and $O_{Asn}$ = O(Asn$_{694}$).

(65) During the review process of this paper, an independent EXAFS study of SLO-1 was published (Scarrow, R. C., Trimitsis, M. G., Buck, C. P., Grove, G. N., Cowling, R. A., Nelson, M. J. *Biochemistry* **1994**, *33*, 15023). The edge and EXAFS analysis of SLO-1 in 50% glycercol from this work and that of the SLO-1$^N$·MeOH of Scarrow *et al.* give very similar first-shell coordination and distances. The results from this work are consistent with the increased intensity of the pre-edge feature and the shorter first-shell distances of SLO-1$^N$ that were observed by Scarrow *et al.* since our MCD results show that the active site of native ferrous SLO-1 in the absence of glycerol is a mixture of five- and six-coordinate forms. However, the five-coordinate species accounts for only ~40% of the sites.

(66) Miller, L. L.; Jacobson, R. A.; Chen, Y.-S.; Kurtz, D. M., Jr. *Acta Crystallogr.* **1989**, *C45*, 527.

(67) Oliver, J. D.; Mullica, D. F.; Hutchinson, B. B.; Milligan, W. O. *Inorg. Chem.* **1980**, *19*, 165.

(68) Kitajima, N.; Fukui, H.; Moro-oka, Y.; Mizutani, Y.; Kitagawa, T. *J. Am. Chem. Soc.* **1990**, *112*, 6402.

(69) Montgomery, H.; Chastain, R. V.; Natt, J. J.; Witkowska, A. M.; Lingafelter, E. C. *Acta Crystallogr.* **1967**, *22*, 775.

(70) Price, D. C. *Can. J. Phys.* **1987**, *65*, 1280.

the four-coordinate structure of Boyington *et al.* (described as a distorted octahedron missing two *cis* ligands). The resulting energy levels are shown in Figure 10A,B,D, respectively.[72]

Comparison of the calculated $^5E_g$ energy levels to those of the experimental $^5E_g$ splittings shows that the five- and six-coordinate LF calculations in Figure 10A,B accurately model the experimentally observed splittings in Figure 7A,B, respectively. The four-coordinate SLO-1 calculations in Figure 10D, which include a span of energies resulting from a reasonable range of LF parameters, show the presence of two transitions in the 5000−13000 $cm^{-1}$ region and an additional high-energy transition at >13 000 $cm^{-1}$. Since the experimental SLO-1 data do not exhibit such high-energy transitions, the four-coordinate crystal structure does not accurately describe the ferrous site in solution. The observed CD/MCD transitions for native ferrous SLO-1 are consistent with the five- and six-coordinate sites in Figure 10A,B. Various spectroscopic techniques have been used to probe the native SLO-1 active site, including magnetic susceptibility,[7] Mössbauer,[15] and EXAFS,[14] all in frozen buffered solution. Since our results indicate that many of the studies were performed on a mixture of five- and six-coordinate sites, with the data interpreted in terms of one site, the previous spectroscopic results must be reconsidered in light of the mixture of sites present for native SLO-1 in solution. For example, the EXAFS results on SLO-1, which have been reinvestigated here in glycerol, give fits different from those previously published[14] for pH 9 sodium borate buffered frozen solution and lyophilized native SLO-1 samples. The previous EXAFS results on SLO-1 in frozen buffered solution[14] gave an iron site surrounded by 2 O's at 1.94 Å and 4 N's at 2.11 Å, while our data support 5 ± 1 O/N at 2.16 Å.

The ferric enzyme has been shown by EPR studies[59,60] to be a mixture of two fairly axial forms with $g$ = 6.2 and 7.4. Addition of alcohols causes the mixture of EPR signals to shift to the clean $g$ = 6.2 peak.[60] The effect of alcohols on our NIR CD/MCD data for the native ferrous SLO-1 site is also dramatic, shifting the mixture of forms to a purely six-coordinate site which has spectral features very similar to those of the six-coordinate component of the native enzyme. The coordination number of the two ferric forms is not known, but MCD studies[73] indicate that a six-coordinate site may also be appropriate for the $g$ = 6.2 species, as it is the only form present when alcohols and glycerol are added to the ferric enzyme. NMR studies[74] of the ferric enzyme showed that alcohols bind near the active site but not directly to the iron, likely in the hydrophobic fatty acid substrate binding site. This may also relate to the alcohol effects on the native ferrous site, which have the same effect as substrate binding to native ferrous SLO-1, and thus the alcohols are likely to bind at the substrate binding site. The substrate effect cannot be studied on the ferric enzyme as it would result in turnover. Thus, the ferric enzyme shows behavior similar to that of the native ferrous enzyme upon addition of alcohols, which may indicate parallel active site coordination between the oxidation states.

$Asn_{694}$ is at the end of a cavity which starts at the surface of the enzyme[6] and which may relate to the fatty acid binding site. It appears that when linoleate (or alcohols) is present at the fatty acid binding site, a change in the active site environment occurs, allowing the Oδ1 of $Asn_{694}$ to bind to the iron, converting the active site to the purely six-coordinate form. Thus, the ferrous SLO-1 plus linoleate substrate form may be the most relevant with respect to catalysis. In the catalytic cycle, ferrous SLO-1 is first oxidized to the active ferric form, which subsequently reacts with substrate, producing product via the radical or organo−iron mechanism. To date the only characterized LO form which is a possible catalytic intermediate is purple LO,[9] which appears to be a ferric hydroperoxo product complex, generated upon addition of excess product or substrate to ferric LOs, and is thought to be the last species in the catalytic cycle. Since the ferric enzyme is eventually reduced upon addition of substrate, it is important to study any intermediates which may be involved with this initial reaction. The effect of anaerobically reducing ferric SLO-1 with substrate was investigated by magnetic susceptibility;[75] however, the results were inconclusive as to any differences between the native ferrous and the substrate-generated ferrous enzyme. A Mössbauer study[76] on the anaerobic reduction of the ferric enzyme with substrate found a quadrupole splitting different from that of native SLO-1, which was attributed to a possible alteration of the active site by oxidation of the native enzyme and subsequent substrate binding. However, in that study, the native enzyme was oxidized by 13-HPOD product and further reacted with linoleic acid in methanol. It is likely that the alcohol or substrate perturbation of the reduced enzyme active site, *i.e.*, the shift from a mixture of five- and six-coordinate forms to pure six-coordination, contributed to the observed Mössbauer quadrupole splittings. Fundamental insight into the mechanism of SLO-1 would require the generation and study of the initial intermediates formed upon addition of substrate to the ferric enzyme and comparison of the electronic and geometric structures to native ferrous SLO-1 in solution.

The NIR CD and MCD studies on the two native mammalian 15-LO active sites show that, in contrast to SLO-1, they exist as purely six-coordinate structures rather than a mixture of five- and six-coordinate sites. XAS pre-edge intensities also indicate that the mammalian 15-LOs are six-coordinate. The edge shapes are also very similar to those of six-coordinate model complexes. The corresponding $Asn_{694}$ amino acid position in SLO-1 is substituted with histidine in rabbit reticulocyte and human 15-LOs.[5] The differences in the spectra of the native plant *vs* these mammalian 15-LOs are reasonably associated with this substitution, as histidine would be a stronger ligand than the carbonyl oxygen of asparagine and lead to a stronger bond. A LF calculation as described above was also performed on the structure in Figure 10C, in which the asparagine O of Figure 10B has been replaced with a histidine N. Comparison of the resulting calculated d-orbital energy levels (Figure 10C) to the experimentally observed transitions for 15-RLO and 15-HLO (Figure 10C,D) shows general agreement for the $^5E_g$ splittings. The calculated $^5T_{2g}$ splittings for both the soybean and mammalian enzymes in Figure 10 are also qualitatively similar to the ground-state splittings obtained through the VTVH MCD analysis (Figure 7), showing a larger $^5T_{2g}$ splitting for the five-coordinate SLO-1 site than for the six-coordinate LOs. It should be noted that the absolute energies of the ground-state levels

(71) Companion, A. L.; Komarynsky, M. A. *J. Chem. Educ.* **1964**, *41*, 257.

(72) Parameters ($\alpha_2$, $\alpha_4$) ($cm^{-1}$) used for the ligand field calculations in Figure 10: (A) five-coordinate SLO-1, short N-His (23 000, 8900), long N-His (21 500, 8500), O-Ile, -$H_{(2)}$O (20 300, 6900); (B) six-coordinate SLO-1, short N-His (16 000, 7000), long N-His (14 940, 4680), O-Ile, -$H_{(2)}$O (13 950, 4650), O-Asn (13 000, 4300); (C) 15-R/HLO, same as (B) but replace O-Asn with N-His (14 900, 4800); (D) four-coordinate crystallographic SLO-1 site, short N-$His_{504,690}$ (19 850, 7850), long N-$His_{499}$ (18 520, 6170), O-$Ile_{839}$ (17 300, 5600).

(73) Zhang, Y.; Gebhard, M. S.; Solomon, E. I. *J. Am. Chem. Soc.* **1991**, *113*, 5162.

(74) Slappendel, S.; Aasa, R.; Falk, K.-E.; Malmström, B. G.; Vänngård, T.; Veldink, G. A.; Vliegenthart, J. F. G. *Biochim. Biophys. Acta* **1982**, *708*, 266.

(75) Petersson, L.; Slappendel, S.; Feiters, M. C.; Vliegenthart, J. F. G. *Biochim. Biophys. Acta* **1987**, *913*, 228.

(76) Funk, M. O., Jr.; Carroll, R. T.; Thompson, J. F.; Sands, R. H.; Dunham, W. R. *J. Am. Chem. Soc.* **1990**, *112*, 5375.

**Scheme 1**

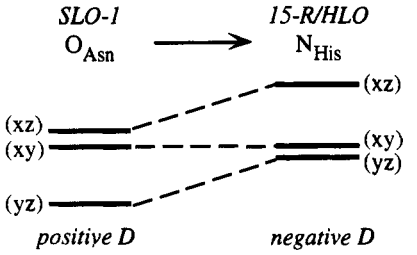


obtained through the LF calculation are overestimated since the method does not include specific $\pi$-bonding effects.

The saturation magnetization data for the mammalian 15-LOs (Figure 6) are qualitatively different from those of the six-coordinate SLO-1 (Figure 4B), exhibiting tighter nesting compared to the plant enzyme data. The VTVH MCD analysis of these data shows that both the five- and six-coordinate sites of SLO-1 have a positive ZFS ($+D$), while the mammalian LOs have a negative ZFS ($-D$). Thus, replacing one ligand on going from the plant to the mammalian enzymes causes large perturbations in the electronic structure of the ferrous site which are clearly exhibited in the behavior of the VTVH MCD data. LF calculations which differ only by the parameters associated with the Asn → His substitution along the molecular $z$-axis (with the asparagine O weaker than the histidine N) reproduce the $+D$ ground-state d-orbital pattern for six-coordinate SLO-1 (Figure 10B, where the two higher-energy components of the $^5T_{2g}$ are closer in energy) and the $-D$ pattern for the mammalian LOs (Figure 10C, where the two lower-energy components are closer). Although one might have expected that the stronger histidine ligand in the mammalian LOs would produce a strong-field $+D$ system and the weaker asparagine ligand in the six-coordinate SLO-1 would produce a weak-field $-D$ system, the opposite is in fact observed and can be explained by examining the nature of the ground-state orbitals obtained from the calculations.

The LF calculations place the $x$-axis as bisecting the two oxygens of Ile and $H_{(2)}O$ in Figure 10 due to the relatively strong ligand field of the *cis* arrangement. These calculations show that the $d_{yz}$ orbital is lowest in energy, followed by the $d_{xy}$ and $d_{xz}$ orbitals for both six-coordinate sites, as shown in Figure 10B,C and in Scheme 1 ($d_{yz}$ and $d_{xz}$ are the predominant components of the lowest and highest of these levels; the "$d_{xy}$" orbital is a mixture of $d_{xy}$ and $d_{x^2-y^2}$). The $d_{yz}$ and $d_{xz}$ orbitals are split in energy due to the asymmetry in the equatorial plane, which contains two *cis* O and two *cis* N ligands. When the weaker asparagine ligand is replaced with the stronger histidine ligand along the $z$-axis, the $d_{xz}$ and $d_{yz}$ orbitals both increase in energy by the same amount, but the $d_{xy}$ orbital remains unchanged. This causes the $d_{xz}$ and $d_{xy}$ orbitals to be closer together and higher in energy than $d_{yz}$ for SLO-1 (Scheme 1, left), corresponding to a strong axial distortion along $x$. For 15-R/HLO, the $d_{yz}$ and $d_{xy}$ orbitals are closer together and lower in energy than $d_{xz}$ (Scheme 1, right), making $y$ a weak axial direction. Since the $x$-axis is a strong axis and the $y$-axis is a weak axis for both six-coordinate LOs, having the primary direction along $x$ produces a $+D$ system for six-coordinate SLO-1 and having the primary direction along $y$ produces a $-D$ system for 15-R/HLO. Therefore, although the spectra of six-coordinate SLO-1 and 15-R/HLO are qualitatively similar, the ground-state VTVH MCD and LF analyses demonstrate significant differences in the electronic structure of the ferrous site between the soybean and mammalian enzymes reasonably ascribed to the Asn → His ligand substitution.

This combination of NIR CD/MCD, VTVH MCD, and XAS spectroscopies has defined the active sites of plant and mammalian 15-LOs, indicating differences in the coordination environment and electronic structure which relate to an Asn → His ligand substitution at the ferrous center. This work is now being extended to study mutants of 15-LOs with systematically varied amino acids which will allow a determination of how specific geometric structural differences in the iron coordination environment affect the electronic structure and reactivity of the LOs.

**Acknowledgment.** This research was supported by grants from the NIH (GM40392, E.I.S., and HL48591, E. Sigal supporting Q.-F.G.) and NSF (CHE-9121576, K.O.H.). We are grateful to Dr. Elliott Sigal, Executive Director of Cell Biology of Syntex Discovery Research, for providing human recombinant 15-LO and rabbit reticulocyte 15-LO and for his input into and support of this study. We also thank Dr. Jim Barnett of Syntex for the preparation of human recombinant 15-LO. Y.Z. gratefully acknowledges Dr. Harold Van Wart, Director of the Institute of Biochemistry and Cell Biology at Syntex, for providing the opportunity and generous support for her work on this project. The Stanford Synchrotron Radiation Laboratory is supported by the Department of Energy, Office of Basic Energy Sciences, Divisions of Chemical Science and Materials Science, and in part by the National Institutes of Health, National Center of Research Resources, Biomedical Research Technology Program (Grant RR-01209, K.O.H.), and the Department of Energy's Office of Health and Environmental Research.

JA943477H